Simulation Analysis of the Carbon Deposition Profile on Directional Material Probes in the Large Helical Device Using the ERO2.0 Code*)

Mamoru SHOJI[1)], Suguru MASUZAKI[1,2)], Gakushi KAWAMURA[1,2)], Juri ROMAZANOV[3)], Andreas KIRSCHNER[3)] and Sebastijan BREZINSEK[3)]

[1)]*National Institute for Fusion Science, National Institutes of Natural Sciences, 322-6 Oroshi-cho, Toki 509-5292, Japan*
[2)]*The Graduate University for Advanced Studies (SOKENDAI), Shonan Village, Hayama 240-0913, Japan*
[3)]*Forschungszentrum Jülich GmbH, Institut für Energie- und Klimaforschung - Plasmaphysik, Partner of the Trilateral Euregio Cluster (TEC), Jülich 52425, Germany*

(Received 19 December 2021 / Accepted 7 February 2022)

The carbon deposition profile on a Directional Material Probe (DMP) installed in the inboard side of the torus in the Large Helical Device (LHD) is investigated using the ERO2.0 code. The experimental result of the carbon deposition profile with short and wide shadows (lower deposition density areas) on the DMP is reasonably explained by the carbons sputtered from the carbon divertor plates installed in the inboard side. The simulation proves that the short and wide shadows are produced by carbons sputtered from the right and left divertor plate arrays, respectively. The experimental carbon deposition profile accumulated in the previous experimental campaign (FY2010) was successfully reproduced by the simulation, which provides detailed understanding of material (carbon) migration in the divertor region in the LHD.

Keywords: ERO2.0, directional material probe (DMP), plasma wall interaction, material migration, EMC3-EIRENE, LHD

DOI: 10.1585/pfr.17.2403010

1. Introduction

Material migration is one of the critical issues for controlling dust particle emission, tritium inventory, and fueling retention in nuclear fusion reactors [1]. In the Large Helical Device (LHD) [2], long pulse plasma discharges have often been interrupted by the emission of large amounts of dust particles from the divertor region. After the experimental campaign, exfoliated carbon-rich mixed material deposition layers were found, which indicated that the exfoliated deposition layers had induced the dust particle emission, leading to interruption of the long pulse plasma discharges [3]. The investigation of material (carbon) migration is an essential issue for controlling the deposition layers in the divertor region.

Directional material probes (DMPs) have been mounted on the surface of the vacuum vessel [4]. The DMP consists of a flat disk and a cylindrical pin, which guides the directionality of incoming particles onto the disk. A DMP was installed on the surface of a helical coil can in the inboard side of the torus in a previous experimental campaign in fiscal year 2010 (FY2010). After this campaign, short and wide shadows (lower deposition density areas) were formed on the disk. The direction of the short shadow was almost perpendicular to the magnetic field line, which suggests that the deposition layer was not produced by impurity ion transport along the magnetic field lines. An analysis using energy dispersive X-ray spectroscopy (EDX) proved that carbon was the dominant material in the deposition layer. It is probable that the deposition layer was formed by neutral carbon atoms sputtered from carbon divertor plates installed in the inboard side near the DMP, which was explained by a simulation using the original Monte-Carlo based plasma wall interaction code ERO [5] in a simple two-dimensional model [6].

The original ERO code has been designed for modeling the plasma wall interactions and three-dimensional impurity transport in the small area on plasma facing components. The simulation volume available is only less than $\sim 1\,\mathrm{m}^3$ which is defined in simple Cartesian coordinates. These constraints in the original ERO code are fatal defects for analyzing the carbon deposition profile on the DMP installed on the three-dimensionally complicated vacuum vessel in the LHD. Therefore, the three-dimensional plasma wall interaction code ERO2.0 was applied [7], which can allow using cylindrical coordinates for flexible definition of the plasma and vacuum vessel geometries. One of the other advantages of ERO2.0 is massive parallelization for obtaining sufficient statistics in larger simulation volumes with a small three-dimensional grid

author's e-mail: shohji.mamoru@nifs.ac.jp

*) This article is based on the presentation at the 30th International Toki Conference on Plasma and Fusion Research (ITC30).

size resolution [8].

In the next section, the setup of a three-dimensional model for the ERO2.0 simulation for analyzing carbon migration in the LHD is shown. In section 3, the simulation of the carbon deposition profile on the DMP is presented with a successful reproduction of the two shadows on the flat disk. In section 4, the experimental result of the carbon density profile on the disk accumulated in the previous experimental campaign is reproduced by the ERO2.0 simulation.

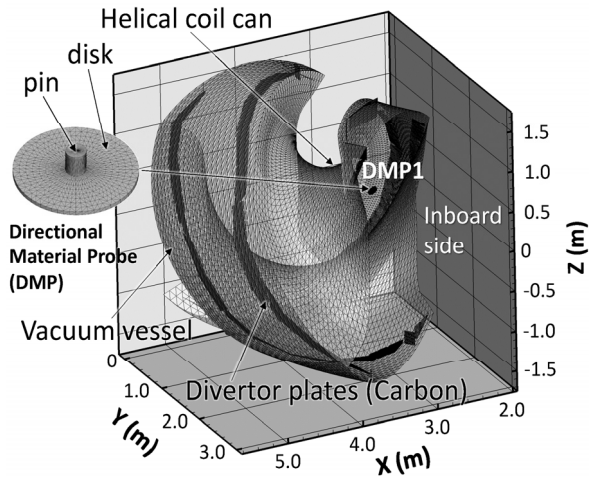

Fig. 1 The three-dimensional model of the open divertor configuration in the LHD for one helical section for analyzing the carbon deposition profile on the DMP by the ERO2.0 simulation.

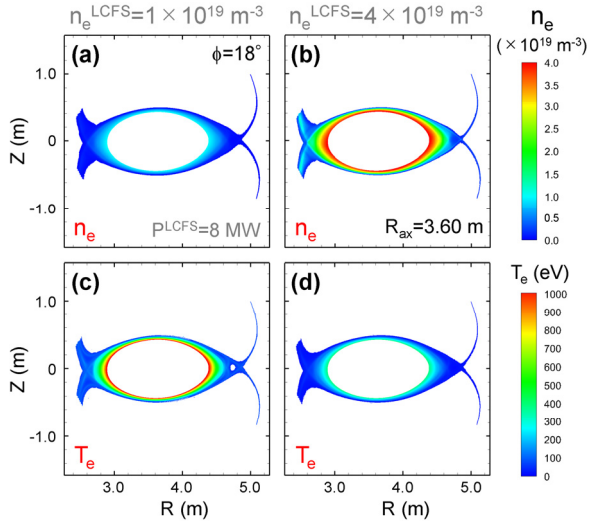

Fig. 2 The poloidal cross-sections of the plasma density profile in a low ($n_e^{LCFS} = 1 \times 10^{19}\,m^{-3}$) (a) and a high ($n_e^{LCFS} = 4 \times 10^{19}\,m^{-3}$) plasma density case (b) with a plasma heating power ($P^{LCFS} = 8\,MW$) for a magnetic configuration ($R_{ax} = 3.60\,m$). The cross-sections of the electron temperature profile for the low (c) and the high (d) plasma densities are also presented.

2. Setup for the ERO2.0 Simulation in the LHD

Figure 1 illustrates a three-dimensional model for the ERO2.0 simulation for the open divertor configuration in the LHD. This model is for one helical section ($0° \le \phi \le 36°$ in the toroidal angle ϕ) in which a periodic boundary condition is assumed at both toroidal ends. A DMP is set on a helical coil can in the inboard side of the torus. The dimension of the DMP is magnified by a factor of four for gaining higher statistical results. It is assumed that the surface on the vacuum vessel is fully covered with carbon, and the DMP is composed of tungsten. A colorimetric analysis of the surface on the vacuum vessel showed that most of the surface was covered with carbon, except for the top of the helical coil can in the inboard side [9]. In this model, the DMP consists of a pin 20 mm in diameter and 22 mm in length, and a flat disk 120 mm in diameter. The temperature of the divertor plates is set to be 600 K. The parameter profile of background hydrogen plasmas is provided by a three-dimensional edge plasma simulation code (EMC3-EIRENE) with a fixed boundary condition of the plasma heating power (P^{LCFS}) and plasma density (n_e^{LCFS}) near the Last Closed Flux Surface (LCFS). The energy and the particle diffusion coefficients in the plasma were assumed to be 0.5 and 1.0 m^2/s, respectively, which are typical values for explaining the measured radial profiles of the electron temperature and the plasma density in the peripheral plasma. Figure 2 shows the poloidal cross-sections (on the R-Z plane) of the plasma density and the electron temperature profiles for low ($n_e^{LCFS} = 1 \times 10^{19}\,m^{-3}$) and high ($n_e^{LCFS} = 4 \times 10^{19}\,m^{-3}$) plasma densities with a plasma heating power ($P^{LCFS} = 8\,MW$). The figure indicates the profiles at a toroidal angle ϕ of 18° where the LHD plasma is horizontally elongated in a typical magnetic configuration where the radial position of the magnetic axis R_{ax} is 3.60 m. In the range of the plasma parameters analyzed in this paper, the EMC3-EIRENE simulations showed no sign of divertor detachment even in high plasma density and low plasma heating power conditions.

3. The Simulation of the Carbon Deposition Profile on the DMP

3.1 Carbon deposition profile for low and high plasma densities

Figures 3 (a) and (b) present the ERO2.0 simulations of the net carbon flux (deposition) density profile on the vacuum vessel for the low and high plasma densities with a plasma heating power ($P^{LCFS} = 8\,MW$) for $R_{ax} = 3.60\,m$, respectively. Although the ERO2.0 code provides a multi-time step solution of the carbon flux density profile, the chained carbon generation on the vacuum vessel caused by the sputtered carbon atoms (self-sputtering) was not included in the simulation for simplicity. The change of the surface material on the DMP due to the carbon deposition

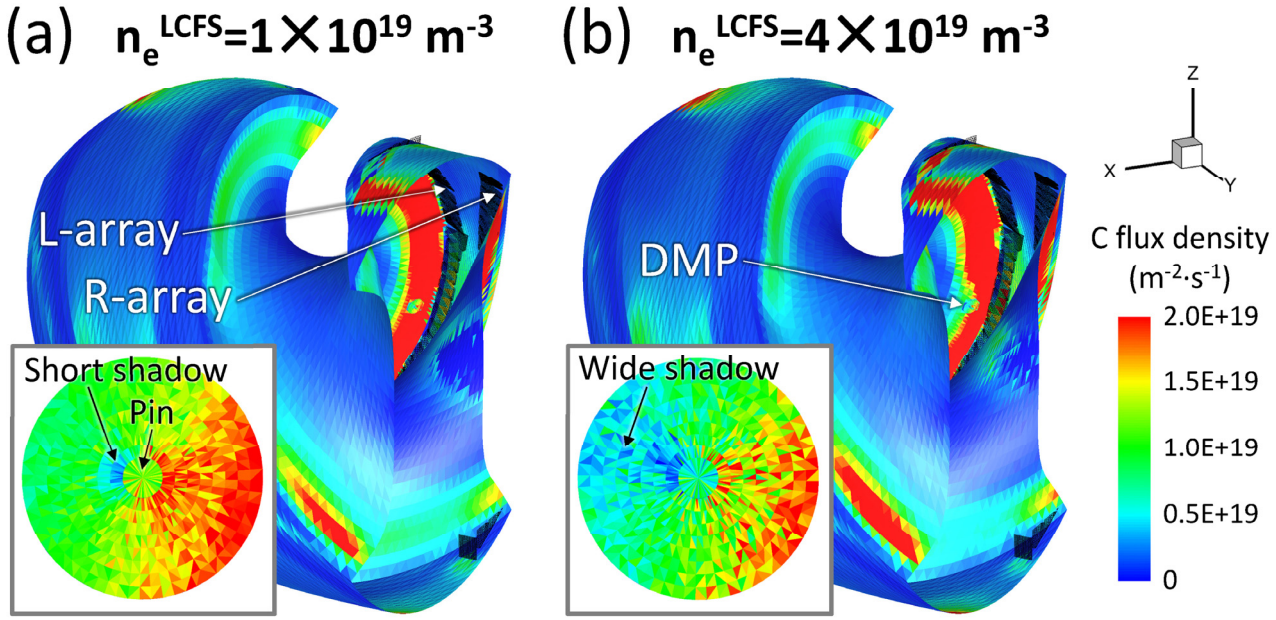

Fig. 3 The ERO2.0 simulation of the carbon flux density profile on the vacuum vessel and the DMP for the low (a) and high (b) plasma densities in the three-dimensional model.

was also not considered, which means that the simulation results correspond to a so-called "the first-time step calculation". The flux of carbons sputtered from the divertor plates was derived from the background plasma parameters (the plasma density, electron and ion temperature, the plasma flow velocity, and the plasma ion flux) on the divertor plates, which are provided by EMC3-EIRENE. The carbon flux also depends on the physical/chemical sputtering coefficients on the divertor plates and the temperature of the divertor plates. The deposited carbon flux density on the surfaces was calculated from the flux, energy, angle of the incoming carbons (hydrocarbons), and the physical/chemical sputtering and reflection coefficients of the surfaces. Figure 3 indicates the high carbon flux density on a side wall of the helical coil can in the inboard side. The insert illustrates the carbon flux density profile on the DMP. For the low plasma density, a short shadow (a lower carbon flux density area) is formed near the pin. For the high plasma density, a wide shadow is produced. These ERO2.0 simulations suggest that the experimental carbon deposition profile on the DMP, which consists of the short and wide shadows, can be explained by the superposed deposition profile for low and high plasma densities.

3.2 Investigation of the carbon source in the low plasma density

For investigating the carbon source forming the deposition profile on the DMP, the ERO2.0 simulation was performed under a hypothesized condition where the sputtering occurred only on the left or right divertor plate arrays in the inboard side. Figure 4 (a) presents the simulation of the carbon deposition profile on the vacuum vessel for the low plasma density when the sputtering occurred only on the left divertor plate array. The simulation in this hypothesized condition shows the high carbon flux density on the surface of the helical coil can, which also presents the carbon deposition profile on the DMP with a wide shadow which was formed by the carbons sputtered from the left divertor plate array. Figure 4 (b) gives the simulation of the deposition profile on the vacuum vessel which included sputtering only on the right divertor plate array. The carbon flux density around the DMP was higher than that in the other regions because of the short distance between the DMP and the right divertor plate array near the equatorial plane. The deposition profile on the DMP presented a short shadow. The simulation reveals that the short shadow was formed by the carbons sputtered from the right divertor plate array. The lower carbon flux density on the DMP compared to that on the vacuum vessel in the proximity is due to the difference of the material on the surfaces. In the ERO2.0 simulation, it is assumed that the surface on the vacuum vessel was carbon which particle reflection coefficient is lower than that of tungsten (the material of the DMP). The lower reflection coefficient of carbon provides the higher carbon flux density deposited on the surface of the vacuum vessel [10].

3.3 Investigation of the carbon source in the high plasma density

Figure 5 (a) gives the simulation of the carbon flux density profile for the high plasma density in a case where sputtering only on the left divertor plate array is considered. The simulation shows high carbon flux density on the helical coil can and the wide shadow on the DMP which

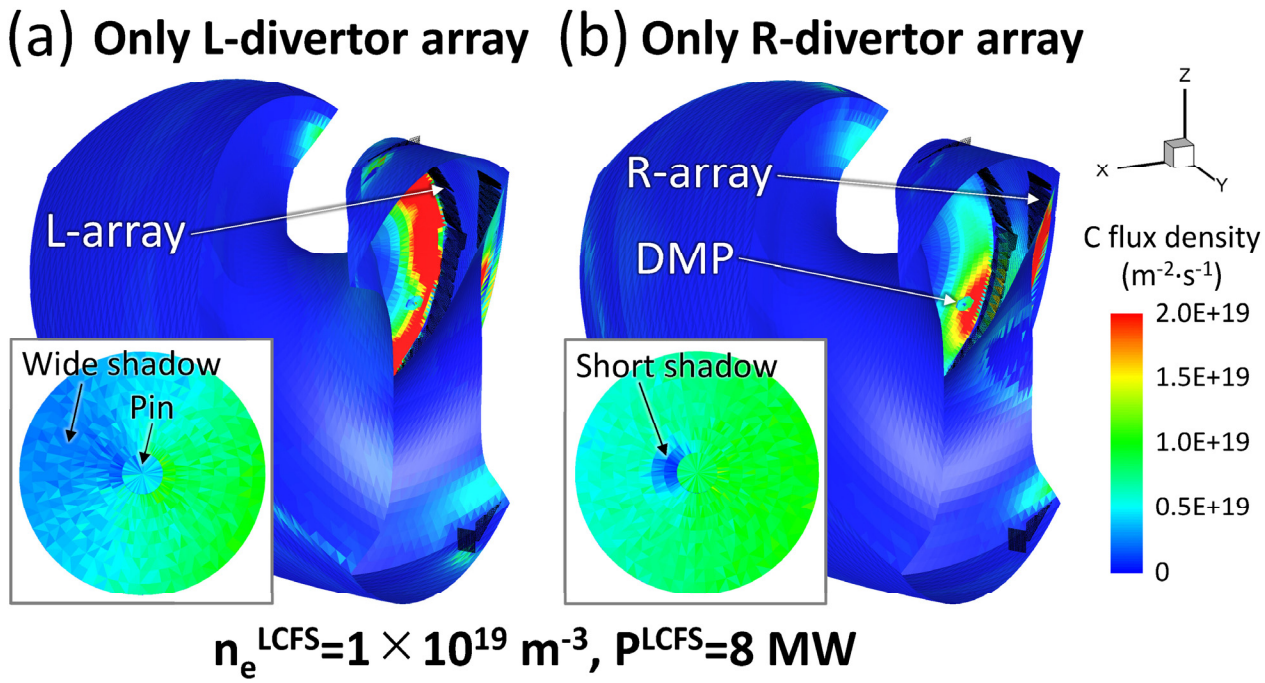

Fig. 4 The simulation of the carbon flux density profile on the vacuum vessel and the DMP for the low plasma density in which the sputtering only on the left (a) and the right (b) carbon divertor plate arrays was included.

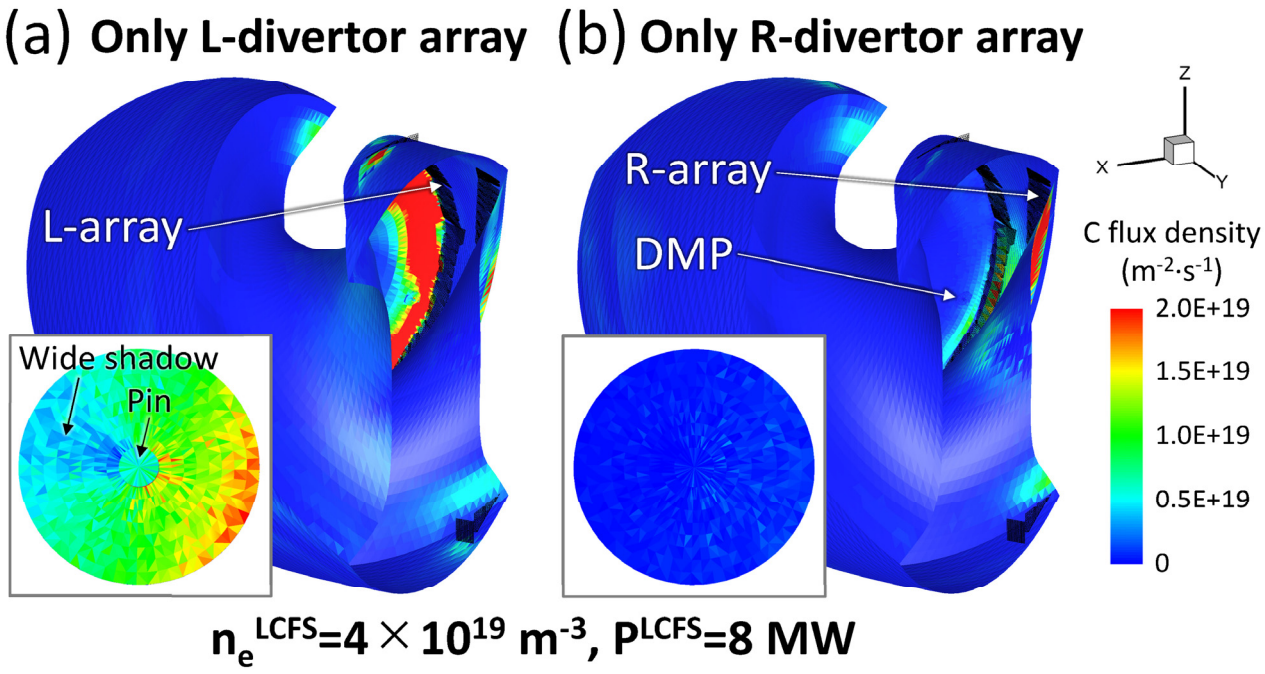

Fig. 5 The simulation of the carbon flux density profile on the vacuum vessel and the DMP for the high plasma density in which the sputtering only on the left (a) and the right (b) carbon divertor plate arrays was included.

were formed by sputtering from the left divertor plate array. Figure 5 (b) depicts the carbon flux density profile in a case including sputtering only on the right divertor plate array. Being different from the simulation for the low plasma density shown in Fig. 4 (b), the carbon flux density on the helical coil can was significantly low, and the carbon deposition on the DMP was negligible. The reason for the low carbon deposition was due to the ionization of carbon atoms sputtered from the right divertor plate array because of the high plasma density in the divertor legs in the inboard side. The background plasma parameter profiles calculated by EMC3-EIRENE showed that the

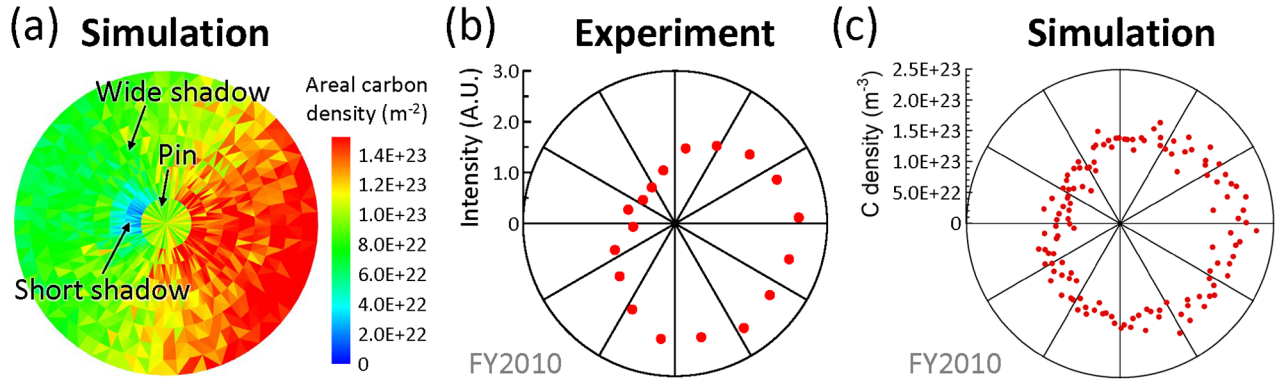

Fig. 6 (a) The ERO2.0 simulation of the areal carbon flux density profile on the DMP accumulated in the previous experimental campaign (FY2010), (b) the pie chart showing the experimental result of the characteristic X-ray intensity of carbon on the DMP along the circumference of the circle having the half radius of the disk, and (c) the pie chart of the simulation of the carbon flux density along the circumference of the circle on the DMP accumulated in the previous experimental campaign.

typical plasma density and electron temperature on the divertor legs in the inboard side around the equatorial plane are $\sim 1 \times 10^{18}\,\mathrm{m}^{-3}$, $\sim 100\,\mathrm{eV}$ for the low plasma density, and $\sim 1 \times 10^{19}\,\mathrm{m}^{-3}$, $\sim 20\,\mathrm{eV}$ for the high plasma density, respectively. The mean free path of the neutral carbon atoms sputtered from the divertor plates for the low and high plasma densities is derived from the rate coefficient of an electron impact ionization of neutral carbon atoms ($C + e^- \rightarrow C^+ + 2e^-$) and the velocity of sputtered carbon atoms. The rate coefficients are obtained from atomic and molecular numerical databases in NIFS [11]. The velocity of the sputtered carbon atoms was calculated by ERO2.0. The mean free paths of the carbon atoms in the divertor legs are estimated to be $\sim 0.16\,\mathrm{m}$ and $\sim 0.01\,\mathrm{m}$ in the low and the high plasma density cases, respectively. These results are reasonable to explain the low carbon deposition on the DMP for the high plasma density (shown in Fig. 5 (b)). The carbons sputtered from the right divertor plate array are mostly ionized before reaching the DMP in the divertor legs where the width of the plasma is more than $\sim 0.03\,\mathrm{m}$ in the most typical magnetic configuration ($R_{\mathrm{ax}} = 3.60\,\mathrm{m}$).

4. Comparison of the Simulation with the Experimental Deposition Profile on the DMP

For validating the ERO2.0 code, the simulation of the carbon deposition profile on the DMP accumulated in plasma discharge conditions for the previous experimental campaign was compared with the experimental result. The simulation was obtained by summing up the carbon flux density deposited on the DMP in various operational conditions performed in the previous experimental campaign. The plasma discharge time was classified by the plasma heating power P^{LCFS}, plasma density $n_{\mathrm{e}}{}^{\mathrm{LCFS}}$, and the magnetic configuration R_{ax}. The plasma heating power, and the plasma density were classified into five ones such as $P^{\mathrm{LCFS}} = 1, 2, 4, 6, 8\,\mathrm{MW}$, and $n_{\mathrm{e}}{}^{\mathrm{LCFS}} = 1, 2, 4, 6, 8 \times 10^{19}\,\mathrm{m}^{-3}$, respectively. The magnetic configuration was classified into three typical ones such as $R_{\mathrm{ax}} = 3.60, 3.75, 3.90\,\mathrm{m}$. As a result, the total number of the classified operational conditions was $5 \times 5 \times 3 = 75$. This classification showed that the total plasma discharge time in the previous experimental campaign was 18567 sec., and the discharge times for the three typical magnetic configurations and other ones were 11898, 4162, 1795, and 712 sec., respectively. Using the classified discharge times and the simulations of the carbon flux density profiles in the experimental conditions, the areal carbon flux density profile on the DMP was obtained, as shown in Fig. 6 (a). In this analysis, the carbon flux density for the other magnetic configurations was not included because of the short total discharge time. The simulation clearly demonstrates the directionality of the carbon deposition profile, which reasonably reproduces the experimental result with the short and wide shadows. Figure 6 (b) is the pie chart indicating the measured intensity profile of the characteristic X-ray of carbon, which is proportional to the areal carbon density along the circumference of the circle, having a radius of 7.5 mm, which corresponds to the half radius of the disk. Figure 6 (c) is the pie chart presenting the simulation of the carbon flux density profile along the circumference. The simulation also presents the directionality (asymmetry) of the carbon deposition density profile on the DMP, which is consistent with the measured carbon flux density profile.

5. Summary

The directionality of the carbon density profile deposited on the DMP installed in the inboard side of the torus was found in the previous experimental campaign (FY2010). The carbon deposition profile showed short and wide shadows (lower deposition U areas) on the flat disk. The ERO2.0 simulations revealed that the wide shadow was formed by the carbons sputtered from the left divertor

plate array in the inboard side, and the short shadow was produced by the carbons sputtered from the right divertor plate array. The experimental result on the DMP in the previous experimental campaign was reasonably explained by the simulation, which demonstrates that the ERO2.0 is applicable to the detailed study of carbon migration in the divertor region in the LHD.

Acknowledgments

This work was performed under the auspices of the NIFS Collaboration Research program (NIFS 20KNSP007). One of the authors (M.S.) appreciates the computational resources of the plasma simulator in NIFS. This work is also supported by JSPS KAKENHI Grant Numbers 18H01203, and 21K18620.

[1] M. Shimada *et al.*, J. Nucl. Mater. **438**, S996 (2013).
[2] Y. Takeiri *et al.*, Nucl. Fusion **57**, 102023 (2017).
[3] M. Shoji *et al.*, Nucl. Fusion **55**, 053014 (2015).
[4] S. Masuzaki *et al.*, Plasma Fusion Res. **8**, 1202110 (2013).
[5] A. Kirschner *et al.*, Nucl. Fusion **40**, 989 (2000).
[6] G. Kawamura *et al.*, Contrib. Plasma Phys. **50**, 451 (2010).
[7] J. Romazanov *et al.*, Nucl. Mater. Energy **18**, 331 (2019).
[8] J. Romazanov *et al.*, Phys. Scr. **T170**, 014018 (2017).
[9] G. Motojima *et al.*, Plasma Fusion Res. **10**, 1202074 (2015).
[10] W. Eckstein, "Calculated Sputtering, Reflection and Range Values", IPP-Report **9**/132 (2002).
[11] NIFS DATABASE http://dbshino.nifs.ac.jp